Journal of Materials Chemistry B

ROYAL SOCIETY OF CHEMISTRY

PAPER

View Article Online
View Journal | View Issue

Cite this: J. Mater. Chem. B, 2024, 12, 2324

Pretargeted radiotherapy and synergistic treatment of metastatic, castration-resistant prostate cancer using cross-linked, PSMA-targeted lipoic acid nanoparticles†

Liqun Dai,‡[a] Xiaoyang Zhang,‡[be] Siming Zhou,[a] Jie Li,[a] Lili Pan,[b] Chunyan Liao,[c] Zhipeng Wang,[d] Ying Chen,[c] Guohua Shen,[b] Lin Li,[b] Rong Tian,[b] Hongbao Sun,[a] Zhenhua Liu,*[d] Shiyong Zhang*[c] and Haoxing Wu*[a]

Metastatic castration-resistant prostate cancer (CRPC) is a currently incurable disease associated with high mortality. Novel therapeutic approaches for CRPC are urgently needed to improve prognosis. In this study, we developed cross-linked, PSMA-targeted lipoic acid nanoparticles (cPLANPs), which can interact with transmembrane glycoprotein to accumulate inside prostate cancer cells, where they upregulate caspase-3, downregulate anti-apoptotic B-cell lymphoma-2 (BCL-2), and thereby induce apoptosis. The *trans*-cyclooctene (TCO) decoration on cPLANPs acts as a bioorthogonal handle allowing pretargeted single-photon emission computed tomography and radiotherapy, which revealed significantly enhanced tumor accumulation and minimal off-target toxicity in our experiments. The developed strategy showed a strong synergistic anti-cancer effect *in vivo*, with a tumor inhibition rate of up to 95.6% after 14 days of treatment. Our results suggest the potential of combining bioorthogonal pretargeted radiotherapy with suitable PSMA-targeted nanoparticles for the treatment of metastatic CRPC.

Received 27th October 2023,
Accepted 1st February 2024

DOI: 10.1039/d3tb02543h

rsc.li/materials-b

Introduction

Prostate cancer is the second most common malignancy and the fifth leading cause of cancer-related death among men worldwide.[1,2] Metastatic castration-resistant prostate cancer (mCRPC) is the most lethal stage of prostate cancer, and it is associated with poor prognosis.[3] Recent years have witnessed tremendous progress in the treatment of mCRPC, involving mostly second-generation androgen receptor (AR)-targeted therapy, cytotoxic chemotherapy, poly (ADP-ribose) polymerase (PARP) inhibition, prostate-specific membrane antigen (PSMA)-targeting therapy, *etc.*[4] Although these novel agents have improved the prognosis of patients with advanced prostate cancer to a certain extent, drug resistance inevitably occurs, necessitating the continuous exploration of novel therapeutic strategies and targets.

PSMA is a type II transmembrane glycoprotein strongly expressed in the malignant prostate epithelium but weakly expressed in benign prostate and non-prostate tissues.[5,6] PSMA can be internalized by prostate cancer cells, enabling it to deliver molecular agents within cells, where they can exert highly specific and efficient anti-tumor effects.[7,8] In the VISION trial, the PSMA-targeted radioligand agent ^{177}Lu-PSMA-617 (Pluvicto) delivered beta-particle radiation to PSMA-positive cells, significantly delaying tumor progression and prolonging survival for patients with mCRPC.[9] Thus, PSMA has been recognized as a "game changer" in the development of effective mCRPC treatments.

In addition to PSMA, the B-cell lymphoma-2 (BCL-2) protein family is another promising target for treating prostate cancer. Anti-apoptotic BCL-2 proteins regulate intrinsic apoptosis in mitochondria and they are overexpressed in many types of tumors,[10–16] including CRPC.[17] High expression of BCL-2 has been linked to resistance to androgens and chemotherapeutic drugs.[18,19] The expression of pro- and anti-apoptotic BCL-2 proteins is modulated by various cellular stressors such as energy stress, DNA damage, growth factor withdrawal, and

[a] Department of Nuclear Medicine and Huaxi MR Research Center (HMRRC), Functional and Molecular Imaging Key Laboratory of Sichuan Province and Frontiers Science Center for Disease Related Molecular Network, West China Hospital, Sichuan University, China. E-mail: haoxingwu@scu.edu.cn
[b] Department of Nuclear Medicine, West China Hospital, Sichuan University, 37 Guoxue Alley, Chengdu 610041, Sichuan, China
[c] College of Biomedical Engineering and National Engineering Research Center for Biomaterials, Sichuan University, 29 Wangjiang Road, Chengdu 610064, China. E-mail: szhang@scu.edu.cn
[d] Department of Urology, Institute of Urology, West China Hospital, Sichuan University, Chengdu, China. E-mail: zhliu@scu.edu.cn
[e] Department of Nuclear Medicine, The First Affiliated Hospital of Chongqing Medical University, Chongqing 400016, China

† Electronic supplementary information (ESI) available. See DOI: https://doi.org/10.1039/d3tb02543h

‡ L. D. and X. Z. contributed equally.

hypoxia.[11] One way to downregulate anti-apoptotic BCL-2 proteins may be α-lipoic acid (LA), a B vitamin with anti-oxidant properties. LA has been widely used to develop highly biocompatible drug carriers.[20–22] In cancer cells, LA and its reduced form dihydrolipoic acid (DHLA) upregulate caspase-3 and downregulate anti-apoptotic BCL-2 proteins, promoting cancer cell apoptosis through the mitochondrial pathway.[23–25]

On the other hand, although β-emitting radiotherapy is a powerful tool for cancer treatment,[26] it suffers from undesirable off-target toxicity. For example, ^{177}Lu-PSMA-617 induces bone marrow toxicity and xerostomia due to its internalization in the salivary glands.[7,27] The bioorthogonal pretargeting strategy using the tetrazine (Tz) chemistry has emerged as a promising approach for delivering radiotracer *in vivo* to improve the tumor-non tumor ratio in molecular imaging.[28–33]

Based on the evidence mentioned above, we herein suggest a synergistic cell-type-specific apoptosis and pretargeted β-emitting radiotherapy approach for treating mCRPC using a rational designed cross-linked PSMA-targeted LA-based nanoparticles (cPLANPs). For the preparation of cPLANPs, an amphiphilic precursor was first synthesized by conjugating *N*-[*N*-[(*S*)-1,3-dicarboxypropyl]carbamoyl]-(*S*)-lysine (DCL) with an LA moiety through a TCO functionalized lysine linker. The PSMA-targeted lipoic acid amphiphile (PLAA) was then readily self-assembled into nanoparticles under aqueous conditions, which were cross-linked upon ultraviolet (UV) irradiation.[34] Hydrophilic DCL endowed the nanoparticles with PSMA-targeting ability, while the hydrophobic LA and TCO components provided them anti-cancer potency *via* BCL-2 targeting and bioorthogonal pretargeting capability respectively. After the circulating nanoparticles had accumulated at tumor sites, a ^{131}I-labeled Tz derivative ([^{131}I]Tz) was administered, and it conjugated selectively with TCO at the tumor site whereas it was rapidly cleared from normal tissues, enabling pretargeted single-photon emission computerized tomography (SPECT) imaging and radiotherapy with significantly enhanced signal-to-background ratio and reduced radiation damage to normal tissues (Scheme 1). Through a parallel, synergistic therapeutic pathway, cPLANPs easily disassembled in cancer cells overexpressing glutathione (GSH), and LA was converted into DHLA by glutathione and thioredoxin reductases, leading to cell apoptosis *via* down-regulation of BCL-2 and upregulation of caspase-3.

Results and discussion

Design, synthesis, and characterization of cPLANPs.

PLAA was synthesized in 24% yield through a four-step process using commercially available DCL and LA (ESI†). First, DCL was conjugated with a hydrophobic LA moiety through a lysine linker *via* two amide bonds. DCL has a canonical PSMA-targeting

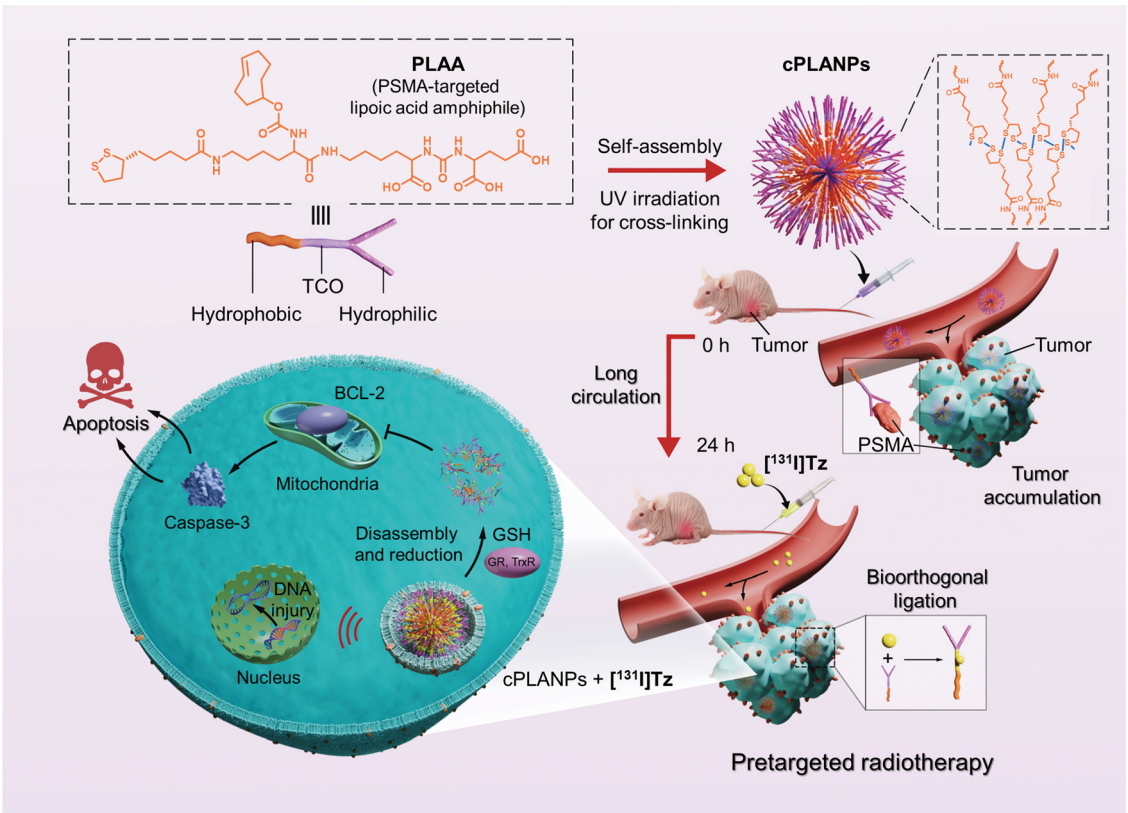

Scheme 1 Schematic illustration of the preparation of cross-linked, PSMA-targeted, LA-based nanoparticles (cPLANPs) and the synergistic anti-cancer mechanism of cPLANPs-based, pretargeted radiotherapy. BCL-2, B-cell lymphoma-2; GR, glutathione reductase, GSH, glutathione; PSMA, prostate-specific membrane antigen; TCO, *trans*-cyclooctene; TrxR, thioredoxin reductase.

structure that consists in several promising radiolabeled ligands for targeted imaging or clinical treatment of prostate cancer, and it bears multiple carboxylic acid groups that offer high hydrophilicity.[35] The branched amino group of the lysine linker was also conjugated with a bioorthogonal TCO tag, affording the desired PLAA molecule, which readily self-assembled into nanoparticles above the critical aggregation concentration of 2.1 mM in phosphate-buffered saline (PBS) (Fig. S2, ESI†). Moreover, UV irradiation was applied to induce ring-opening disulfide exchange polymerization for subsequent cross-linking.

Transmission electron microscopy (TEM) and dynamic light scattering (DLS) revealed that cPLANPs had a spherical morphology with a diameter of 55 nm and a hydrodynamic diameter of 64.9 nm (Fig. 1A and B). Consistent with a previous study,[21] the zeta potential of cPLANPs at pH 7.2 was around −38.1 mV, which increased to −17.4 mV at pH 6.5 and to 0.09 mV at pH 5.5 in RPMI-1640 supplemented with 10% fetal bovine serum (FBS) (Fig. 1C). This is attributed to reduced ionization of the carboxylic acid groups at the surface of cPLANPs under lower pH conditions, resulting in less negative charges. These results suggest that cPLANPs can be internalized efficiently under the mildly acidic conditions of the tumor microenvironment. DLS also revealed that nanoparticle size was not considerably affected over time during incubation in RPMI-1640 by itself (Fig. S3, ESI†) or supplemented with 10% FBS (Fig. 1D), even at cPLANPs concentrations down to 10 μg mL^{-1}. These results suggest stability of cPLANPs under physiological conditions.

In vitro anti-cancer activity of cPLANPs.

The effect of cPLANPs on cell viability was assessed in PSMA-positive LNCaP cells, PSMA-negative PC3 cells, and MSC cells as a normal control. No significant decrease was observed in the viability of normal or PC3 cells after 24-h treatment with 1–500 μg mL^{-1} cPLANPs (Fig. S4, ESI†). In contrast, the viability of LNCaP cells decreased gradually over time in a dose-dependent manner (Fig. 2A): treatment with 50–500 μg mL^{-1} cPLANPs significantly reduced viability at 24 h, while viability was reduced at 48 and 72 h even at the lowest cPLANPs concentrations tested. Flow cytometry after 48-h treatment confirmed that cell apoptosis increased with increasing nanoparticle concentration (Fig. 2C). These results indicate that tumor cells internalized the PSMA-targeted cPLANPs.

Since cPLANPs disassemble in GSH-overexpressing tumor cells, we also measured cell viability in culture medium supplemented with 10 mM GSH as an *in vitro* model of the tumor microenvironment. Treatment with cPLANPs significantly reduced the viability of LNCaP cells in a dose-dependent manner (Fig. 2B), and the cytotoxic effect was stronger and faster than in RPMI-1640 lacking GSH. For example, treating cells with 200 μg mL^{-1} cPLANPs reduced cell viability to 70% at 24 h, 64% at 48 h, and 61% at 72 h, whereas the corresponding values in the absence of GSH were 92%, 82% and 73%. To elucidate the mechanism underlying the anti-tumor effect of the developed nanoparticles, LNCaP cells were treated with 0–1000 μg mL^{-1} cPLANPs for 48 h, and the expression of BCL-2 and caspase-3 was evaluated by Western blotting (Fig. 2D). cPLANPs significantly downregulated BCL-2 at concentrations above 50 μg mL^{-1} (Fig. 2E), while they significantly upregulated caspase-3 at concentrations above 50 μg mL^{-1} (Fig. 2F), in a dose-dependent manner in both cases. Experiments were also performed in C4-2 cells, which is androgen-independent. In consistence with the results in LNCaP cells, cPLANPs also significantly downregulated BCL-2 and upregulated caspase-3 in C4-2 cells at concentrations above 50 μg mL^{-1}, in a dose-dependent manner (Fig. 2G–I). These

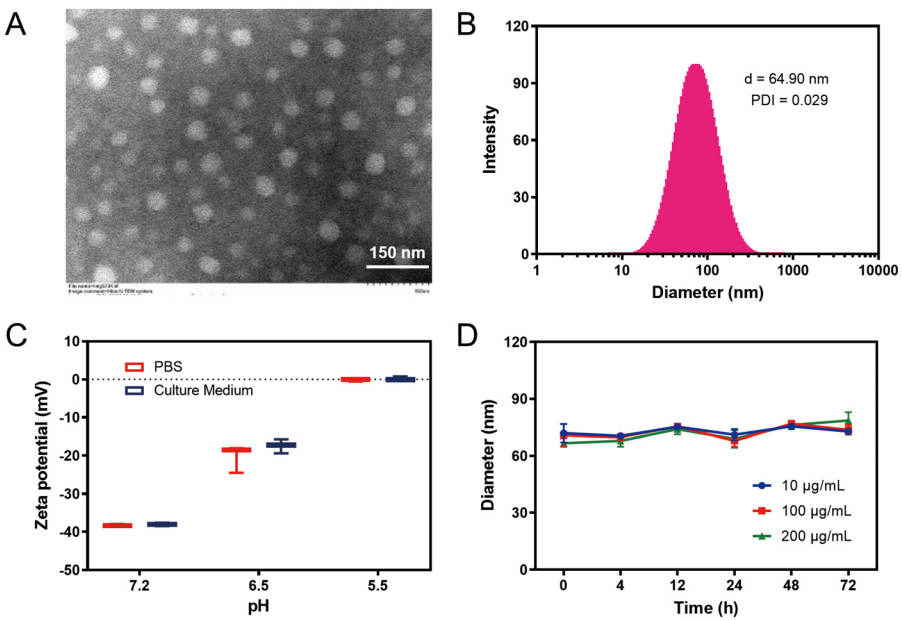

Fig. 1 Characterization of cross-linked, PSMA-targeted, lipoic acid nanoparticles. (A) Transmission electron microscopy imaging. (B) Dynamic light scattering analysis. (C) Zeta potential at different pH values. (D) *In vitro* stability in RPMI-1640 supplemented with 10% fetal bovine serum at 25 °C. PBS, phosphate-buffered saline; PDI, polydispersity index.

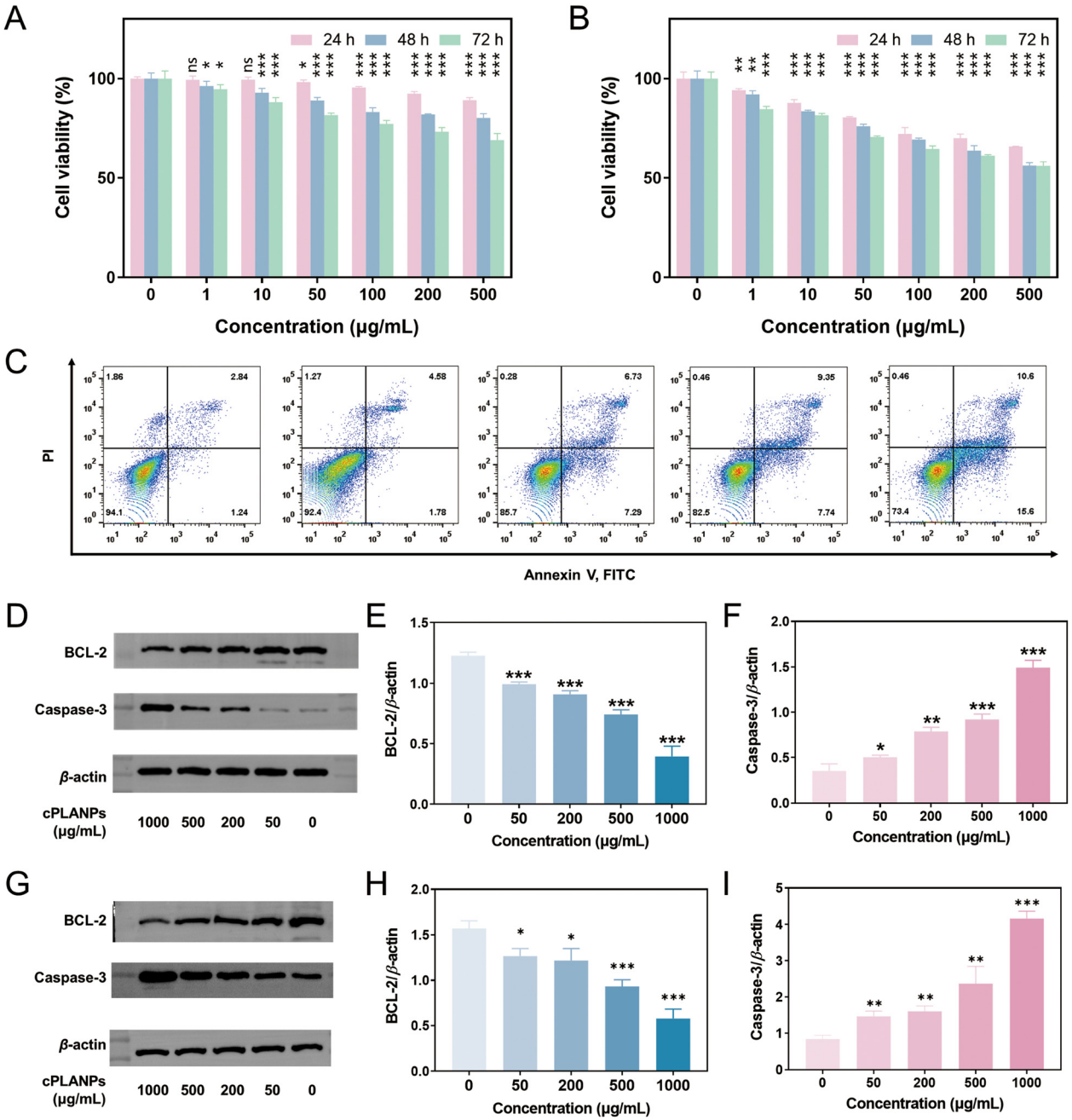

Fig. 2 *In vitro* anti-cancer activity of cross-linked, PSMA-targeted, lipoic acid nanoparticles (cPLANPs). (A) and (B) Viability of LNCaP cells after treatment with 1–500 μg mL^{-1} cPLANPs lasting 24, 48, or 72 h in RPMI-1640 medium (A) by itself or (B) supplemented with 10 mM glutathione. (C) Apoptosis of LNCaP cells after 48-h treatment with cPLANPs at concentrations of, from left to right, 0, 10, 50, 100, or 200 μg mL^{-1}. Cells were stained with PI/annexin V-FITC, then analyzed by flow cytometry. (D) Representative Western blots against B-cell lymphoma-2 (BCL-2) and caspase-3 in LNCaP cells. (E) and (F) Relative expression of (E) BCL-2 and (F) caspase-3 in LNCaP cells, normalized to levels of actin. (G) Representative Western blots against BCL-2 and caspase-3 in C4-2 cells. (H) and (I) Relative expression of (H) BCL-2 and (I) caspase-3 in C4-2 cells, normalized to levels of actin. FITC, fluorescein isothiocyanate; PI, propidium iodide. *$p < 0.05$, **$p < 0.01$, ***$p < 0.001$.

results suggest that the developed nanoparticles promote cancer cell apoptosis through the mitochondrial pathway *via* a pro-oxidative mechanism, consistent with the reported mechanism of LA-induced cell apoptosis.[20,21]

Simulation of cPLANPs-based pretargeted radiotherapy *in vitro*

The cellular uptake of cPLANPs was visualized by pretargeted fluorescence imaging. Strong fluorescence was observed in LNCaP cells that had been sequentially incubated with cPLANPs (10 ng mL^{-1}) and a Tz-modified fluorescent probe (**Tz-Cy5**) (Fig. 3A), whereas negligible signal was detected in PC3 cells or PSMA-blocked LNCaP cells (Fig. 3B). Similar results were observed in C4-2 cells (Fig. S13, ESI†). These results indicate that cPLANPs, even at low concentrations, can be efficiently internalized by PSMA-positive cells, and that target tumors contain a sufficient

amount of TCO for intracellular bioorthogonal ligation, which is essential for *in vivo* pretargeted nuclear imaging and radiotherapy.

The anti-cancer efficacy of cPLANPs-based, pretargeted radiotherapy was simulated *in vitro* using **[^{131}I]Tz** (Fig. 3A) as a radioligand with favorable radiochemical yield (76%). LNCaP

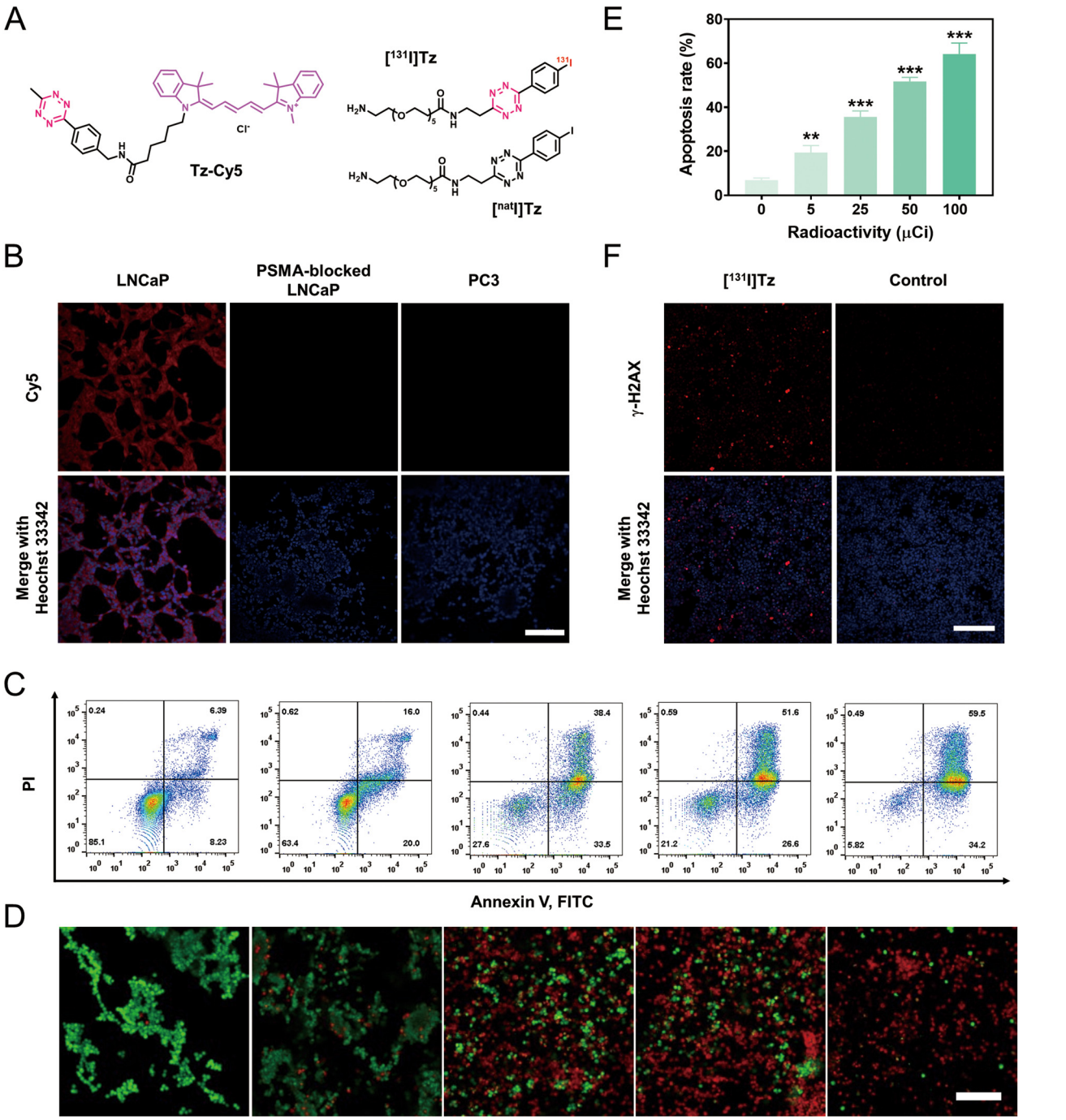

Fig. 3 Simulation of cPLANPs-based, pretargeted radiotherapy *in vitro*. (A) Chemical structures of **Tz-Cy5**, **[^{131}I]Tz** and **[^{nat}I]Tz**. (B) Pretargeted fluorescence imaging of LNCaP and PC3 cells treated with cPLANPs (10 ng mL^{-1}) and **Tz-Cy5** (1 μM). (C) Apoptosis and (D) live-or-dead staining of LNCaP cells treated with cPLANPs (10 ng mL^{-1}) and **[^{131}I]Tz** (left to right: 0, 5, 25, 50, 100 μCi). The cells were first incubated with cPLANPs (10 ng mL^{-1}) for 2 h and washed, then treated with fresh culture medium containing **[^{131}I]Tz** of different radioactivity for 1 h and washed. After another 48 h, the cells were stained for imaging or flow cytometry. (E) Apoptosis rate of LNCaP cells treated with cPLANPs (10 ng mL^{-1}) and increasing concentrations of **[^{131}I]Tz**. $^{**}p < 0.01$, $^{***}p < 0.001$. (F) Immunofluorescence against γ-H2AX in LNCaP cells treated with 10 ng mL^{-1} of cPLANPs by itself (as control) or followed by 100 μCi of **[^{131}I]Tz**. Scale bar, 200 μm. cPLANPs, cross-linked PSMA-targeted lipoic acid-based nanoparticles; FITC, fluorescein isothiocyanate; PI, propidium iodide.

cells were first treated with cPLANPs (10 ng mL^{-1}) for 2 h, washed with PBS to remove free nanoparticles, treated with **[^{131}I]Tz** for 1 h and washed again to remove free **[^{131}I]Tz**. After incubation for another 48 h, flow cytometry was performed. The apoptosis rate increased with **[^{131}I]Tz** radioactivity, from 19.4% at 5 μCi to 64.2% at 100 μCi (Fig. 3C and E). These results were confirmed by live-or-dead cell staining (Fig. 3D). Expression of γ-H2AX, which is a sensitive biomarker of DNA damage, also significantly increased after simulated pretargeted radiotherapy, while negligible expression of γ-H2AX was observed in the control group (Fig. 3F), indicating sufficient DNA damage induced by the simulated pretargeted radiotherapy.

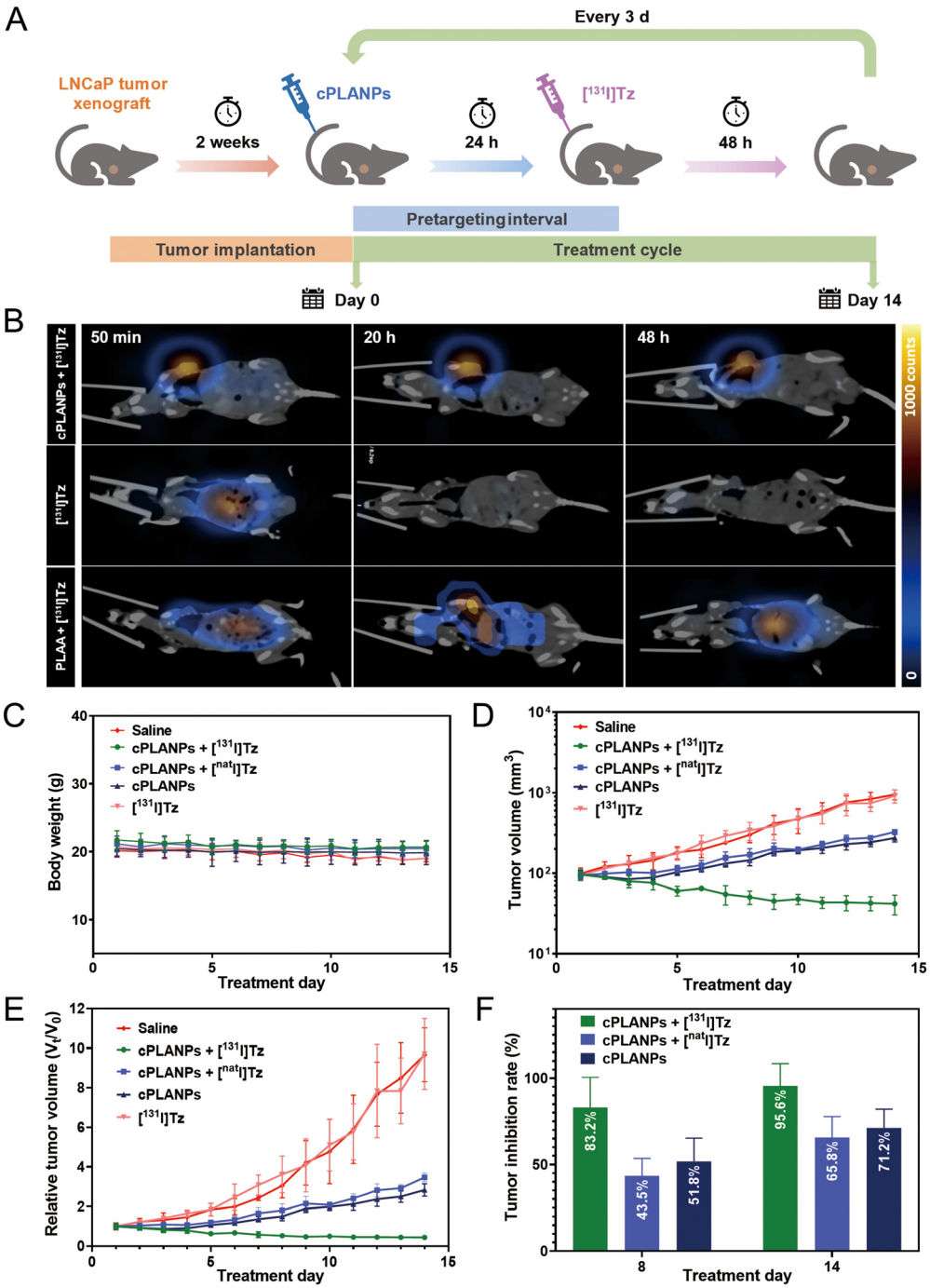

Fig. 4 Single photon emission computed tomography/computed tomography (SPECT/CT) imaging and anti-cancer effect of cPLANPs-based, pretargeted radiotherapy *in vivo*. (A) Schematic illustration of pretargeted radiotherapy in LNCaP tumor-bearing mice. (B) SPECT/CT imaging of mice treated with different formulations at 50 min, 20 h, and 48 h after the injection of **[^{131}I]Tz**. (C and D) Changes in the (C) body weight and (D) tumor volume over time in mice treated with different formulations. (E) Changes in the relative tumor volume over time in each group. (F) Tumor inhibition rate in mice treated with cPLANPs-based formulations. cPLANPs, cross-linked PSMA-targeted lipoic acid-based nanoparticles.

SPECT/CT imaging and anti-cancer effect of cPLANPs-based, pretargeted radiotherapy *in vivo*

The biodistribution of [^{131}I]Tz and its ligation with the biorthogonal TCO moiety on cPLANPs was monitored by SPECT/CT imaging using a LNCaP xenograft mouse model (Fig. 4B). By 40 min post-injection, [^{131}I]Tz had accumulated mainly in the abdomen, and it was rapidly eliminated from the body within 2 h (Fig. S5, ESI†). No significant uptake was observed at the tumor site during imaging. In contrast, significant tumor uptake was observed at 50 min after the administration of

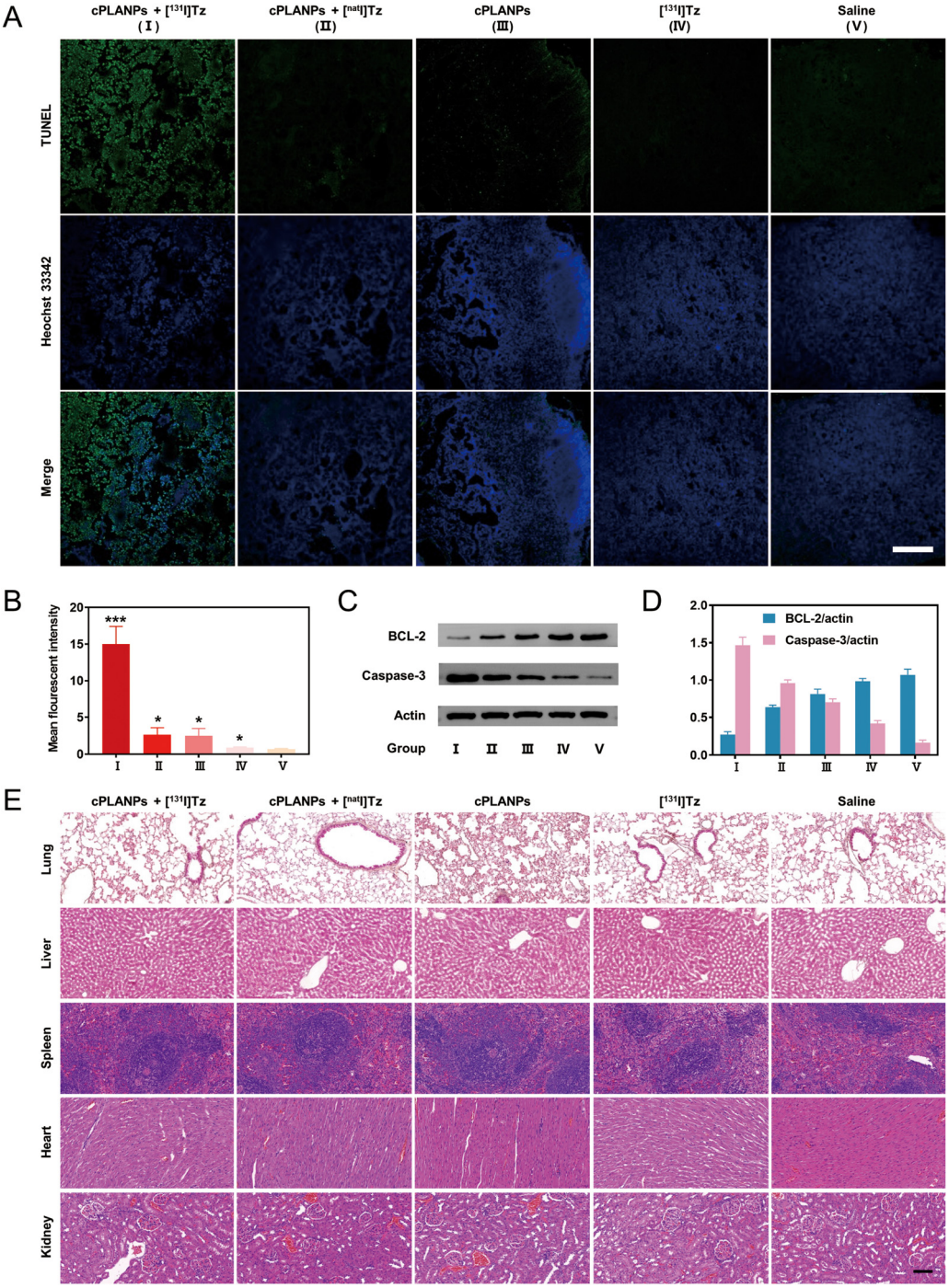

Fig. 5 Synergistic anti-cancer mechanism and safety profile of cPLANPs-based, pretargeted radiotherapy *in vivo*. (A) Tumor sections from LNCaP tumor-bearing mice that had been treated with different formulations were subjected to terminal transferase/dUTP nick end labeling (TUNEL) staining. Scale bar, 200 μm. (B) Quantified analysis of TUNEL staining signals. *$p < 0.05$, ***$p < 0.001$. (C) Representative Western blots against B-cell lymphoma-2 (BCL-2) and caspase-3. (D) Relative expression of BCL-2 and caspase-3, normalized to levels of actin. (E) Hematoxylin–eosin staining of major organs collected from LNCaP tumor-bearing mice after the indicated treatment. Scale bar, 100 μm.

[^{131}I]Tz *via* the tail vein in mice that had been pre-injected with cPLANPs 4 h beforehand (cPLANPs + [^{131}I]Tz). These results indicate successful bioorthogonal reaction between [^{131}I]Tz and the active TCO moieties on cPLANPs at the tumor site, where background was negligible in the absence of this reaction. After the bioorthogonal reaction, minimal background radioactivity was observed in tissues outside the tumor, supporting the idea that cPLANPs accumulate selectively in PSMA-positive cancer cells and that free [^{131}I]Tz is rapidly excreted from the body. Tumor uptake remained almost unchanged even by 48 h after the injection of [^{131}I]Tz, indicating the promising radiotherapy potency of this pretargeted strategy. In contrast, the group (PLAA + [^{131}I]Tz) exhibited slow, transient accumulation of radioactivity at the tumor site and substantial off-target distribution, reflecting the lack of efficient bioorthogonal ligation at the tumor site (Fig. 4B).

The synergistic anti-cancer efficacy of cPLANPs-based, pretargeted radiotherapy was assessed in nude mice bearing LNCaP tumors, which were injected with cPLANPs, followed by multiple rounds of [^{131}I]Tz (Fig. 4A). The sequential administration of cPLANPs and [^{131}I]Tz inhibited tumor growth more than other treatments did, giving a tumor inhibition rate of 95.6% after 14 days of treatment (Fig. 4D–F and Fig. S6, ESI†). In contrast, cPLANPs alone or in combination with a tetrazine derivative labeled with a non-radioactive iodine isotope ([^{nat}I]Tz) had a moderate effect on tumor growth (Fig. 4F), reflecting the poor intrinsic anti-cancer activity of cPLANPs. [^{131}I]Tz on its own exerted negligible anti-cancer effects because of its rapid clearance.

To elucidate the mechanism of the anti-cancer effect of cPLANPs-based, pretargeted radiotherapy *in vivo*, tumor sections were collected from mice after various treatments and analyzed using the terminal transferase dUTP nick end-labeling (TUNEL) assay, and Western blotting for expression level of BCL-2 and caspase-3. Consistent with the results from tumor growth inhibition experiments, the fluorescence signal was considerably stronger in the group (cPLANPs + [^{131}I]Tz) than in the groups treated with non-radioactive isotope or cPLANPs, while negligible signal was observed in tumor sections treated with [^{131}I]Tz or saline alone (Fig. 5A and B). Moreover, BCL-2 was downregulated and caspase-3 was upregulated in all cPLANPs-treated groups, and these effects were strongest in the group (cPLANPs + [^{131}I]Tz) (Fig. 5C and D). These results suggest that the anti-cancer effects of cPLANPs *in vivo* involve the formation of DHLA, and they demonstrate that the combined application of cPLANPs and pretargeted radiotherapy can achieve a strong synergistic anti-cancer effect *in vivo*.

The safety profile of cPLANPs-based, pretargeted radiotherapy was assessed by monitoring the body weight of mice during treatment and by staining major organs afterwards with hematoxylin–eosin. None of the treatment groups showed significant differences in body weight from controls (Fig. 4C), nor did they show obvious pathological changes in major organs after 14 days of treatment (Fig. 5E).

Conclusions

A potent synergistic anti-cancer strategy based on cPLANPs was developed. cPLANPs were prepared through an amphiphilic precursor prepared from biogenic LA, PSMA-targeting DCL, and TCO-bearing lysine. The resulting nanoparticles displayed robust stability and demonstrated apoptosis in PSMA-positive cancer cells *via* downregulation of BCL-2 and upregulation of caspase-3. In addition, the bioorthogonal reaction between [^{131}I]Tz and pretargeted cPLANPs at the tumor site facilitated prolonged radiotherapy. After a 14-day treatment period, *in vivo* studies revealed an impressive tumor inhibition rate of up to 95.6%. Our results underscore the great potential of cPLANPs-based pretargeted radiotherapy for the synergistic treatment of mCRPC. Moreover, this method could promise for applications in therapies utilizing other radionuclides, such as ^{177}Lu.

Author contributions

Liqun Dai and Xiaoyang Zhang conceived ideas, conducted experiments, and drafted the original manuscript. Siming Zhou, Jie Li, Lili Pan, Chunyan Liao, Zhipeng Wang, Ying Chen, Guohua Shen, Lin Li, Rong Tian, and Hongbao Sun provided assistance during the experiments. Zhenhua Liu, Shiyong Zhang, and Haoxing Wu revised the manuscript.

Conflicts of interest

There are no conflicts to declare.

Acknowledgements

This work was supported by the National Natural Science Foundation of China (21975165, 81901776, 81971653, and 21907070), the 1.3.5 project for disciplines of excellence at West China Hospital, Sichuan University (ZYYC23003), and Sichuan Science and Technology Innovation Foundation (2021JDTD0015).

References

1 R. L. Siegel, K. D. Miller, H. E. Fuchs and A. Jemal, Cancer statistics, 2022, *CA Cancer J. Clin.*, 2022, **72**(1), 7–33.
2 H. Sung, J. Ferlay, R. L. Siegel, M. Laversanne, I. Soerjomataram, A. Jemal and F. Bray, Global Cancer Statistics 2020: GLOBOCAN Estimates of Incidence and Mortality Worldwide for 36 Cancers in 185 Countries, *CA Cancer J. Clin.*, 2021, **71**(3), 209–249.
3 M. P. Yadav, S. Ballal, R. K. Sahoo, S. N. Dwivedi and C. Bal, Radioligand Therapy With (177)Lu-PSMA for Metastatic Castration-Resistant Prostate Cancer: A Systematic Review and Meta-Analysis, *AJR Am. J. Roentgenol.*, 2019, **213**(2), 275–285.
4 J. Zhang, J. Sun, S. Bakht and W. Hassan, Recent Development and Future Prospects of Molecular Targeted Therapy in Prostate Cancer, *Curr. Mol. Pharmacol.*, 2022, **15**(1), 159–169.
5 D. A. Silver, I. Pellicer, W. R. Fair, W. D. Heston and C. Cordon-Cardo, Prostate-specific membrane antigen

expression in normal and malignant human tissues, *Clin. Cancer Res.*, 1997, **3**(1), 81–85.
6 C. W. Rinker-Schaeffer, A. L. Hawkins, S. L. Su, R. S. Israeli, C. A. Griffin, J. T. Isaacs and W. D. Heston, Localization and physical mapping of the prostate-specific membrane antigen (PSM) gene to human chromosome 11, *Genomics*, 1995, **30**(1), 105–108.
7 N. M. Donin and R. E. Reiter, Why Targeting PSMA Is a Game Changer in the Management of Prostate Cancer, *J. Nucl. Med.*, 2018, **59**(2), 177–182.
8 S. M. Schwarzenboeck, I. Rauscher, C. Bluemel, W. P. Fendler, S. P. Rowe, M. G. Pomper, A. Asfhar-Oromieh, K. Herrmann and M. Eiber, PSMA Ligands for PET Imaging of Prostate Cancer, *J. Nucl. Med.*, 2017, **58**(10), 1545–1552.
9 O. Sartor, J. de Bono, K. N. Chi, K. Fizazi, K. Herrmann, K. Rahbar, S. T. Tagawa, L. T. Nordquist, N. Vaishampayan, G. El-Haddad, C. H. Park, T. M. Beer, A. Armour, W. J. Pérez-Contreras, M. DeSilvio, E. Kpamegan, G. Gericke, R. A. Messmann, M. J. Morris and B. J. Krause, Lutetium-177–PSMA-617 for Metastatic Castration-Resistant Prostate Cancer, *N. Engl. J. Med.*, 2021, **385**(12), 1091–1103.
10 G. Radha and S. C. Raghavan, BCL2: A promising cancer therapeutic target, *BBA – Rev. Cancer*, 2017, **1868**(1), 309–314.
11 A. N. Hata, J. A. Engelman and A. C. Faber, The BCL2 Family: Key Mediators of the Apoptotic Response to Targeted Anticancer Therapeutics, *Cancer Discovery*, 2015, **5**(5), 475–487.
12 P. E. Czabotar, G. Lessene, A. Strasser and J. M. Adams, Control of apoptosis by the BCL-2 protein family: implications for physiology and therapy, *Nat. Rev. Mol. Cell Biol.*, 2014, **15**(1), 49–63.
13 P. N. Kelly and A. Strasser, The role of Bcl-2 and its pro-survival relatives in tumourigenesis and cancer therapy, *Cell Death Differ.*, 2011, **18**(9), 1414–1424.
14 J. Xu, W. Du, Y. Zhao, K. Lim, L. Lu, C. Zhang and L. Li, Mitochondria targeting drugs for neurodegenerative diseases—Design, mechanism and application, *Acta Pharm. Sin. B*, 2022, **12**(6), 2778–2789.
15 S. He, J. Xu, X. Liu and Y. Zhen, Advances and challenges in the treatment of esophageal cancer, *Acta Pharm. Sin. B*, 2021, **11**(11), 3379–3392.
16 M. Li, Y. Wang, M. Li, X. Wu, S. Setrerrahmane and H. Xu, Integrins as attractive targets for cancer therapeutics, *Acta Pharm. Sin. B*, 2021, **11**(9), 2726–2737.
17 Q. Li, Q. Deng, H. P. Chao, X. Liu, Y. Lu, K. Lin, B. Liu, G. W. Tang, D. Zhang, A. Tracz, C. Jeter, K. Rycaj, T. Calhoun-Davis, J. Huang, M. A. Rubin, H. Beltran, J. Shen, G. Chatta, I. Puzanov, J. L. Mohler, J. Wang, R. Zhao, J. Kirk, X. Chen and D. G. Tang, Linking prostate cancer cell AR heterogeneity to distinct castration and enzalutamide responses, *Nat. Commun.*, 2018, **9**(1), 3600.
18 B. J. Feldman and D. Feldman, The development of androgen-independent prostate cancer, *Nat. Rev. Cancer*, 2001, **1**(1), 34–45.
19 B.-H. Choi and H. S. Yoon, FKBP38-Bcl-2 interaction: a novel link to chemoresistance, *Curr. Opin. Pharmacol.*, 2011, **11**(4), 354–359.
20 L. Wang, P. Jing, J. Tan, C. Liao, Y. Chen, Y. Yu and S. Zhang, "One-stitch" bioorthogonal prodrug activation based on cross-linked lipoic acid nanocapsules, *Biomaterials*, 2021, **273**, 120823.
21 C. Liao, X. Dai, Y. Chen, J. Liu, Y. Yao and S. Zhang, Biogenic (R)-(+)-Lipoic Acid Only Constructed Cross-Linked Vesicles with Synergistic Anticancer Potency, *Adv. Funct. Mater.*, 2019, **29**(3), 1806567.
22 J. Huang, L. Wang, P. Zhao, F. Xiang, J. Liu and S. Zhang, Nanocopper-Doped Cross-Linked Lipoic Acid Nanoparticles for Morphology-Dependent Intracellular Catalysis, *ACS Catal.*, 2018, **8**(7), 5941–5946.
23 B. Dörsam and J. Fahrer, The disulfide compound α-lipoic acid and its derivatives: A novel class of anticancer agents targeting mitochondria, *Cancer Lett.*, 2016, **371**(1), 12–19.
24 P. Kafara, P. Icard, M. Guillamin, L. Schwartz and H. Lincet, Lipoic acid decreases Mcl-1, Bcl-xL and up regulates Bim on ovarian carcinoma cells leading to cell death, *J. Ovarian Res.*, 2015, **8**(1), 36.
25 B. Feuerecker, S. Pirsig, C. Seidl, M. Aichler, A. Feuchtinger, G. Bruchelt and R. Senekowitsch-Schmidtke, Lipoic acid inhibits cell proliferation of tumor cells in vitro and in vivo, *Cancer Biol. Ther.*, 2012, **13**(14), 1425–1435.
26 Q. Liu, Y. Qian, P. Li, S. Zhang, Z. Wang, J. Liu, X. Sun, M. Fulham, D. Feng, Z. Chen, S. Song, W. Lu and G. Huang, The combined therapeutic effects of 131iodine-labeled multifunctional copper sulfide-loaded microspheres in treating breast cancer, *Acta Pharm. Sin. B*, 2018, **8**(3), 371–380.
27 C. Kratochwil, W. P. Fendler, M. Eiber, R. Baum, M. F. Bozkurt, J. Czernin, R. C. Delgado Bolton, S. Ezziddin, F. Forrer, R. J. Hicks, T. A. Hope, L. Kabasakal, M. Konijnenberg, K. Kopka, M. Lassmann, F. M. Mottaghy, W. Oyen, K. Rahbar, H. Schoder, I. Virgolini, H. J. Wester, L. Bodei, S. Fanti, U. Haberkorn and K. Herrmann, EANM procedure guidelines for radionuclide therapy with (177)Lu-labelled PSMA-ligands ((177)Lu-PSMA-RLT, *Eur. J. Nucl. Med. Mol. Imaging*, 2019, **46**(12), 2536–2544.
28 A. Rondon and F. Degoul, Antibody Pretargeting Based on Bioorthogonal Click Chemistry for Cancer Imaging and Targeted Radionuclide Therapy, *Bioconjug. Chem.*, 2020, **31**(2), 159–173.
29 B. L. Oliveira, Z. Guo and G. J. L. Bernardes, Inverse electron demand Diels-Alder reactions in chemical biology, *Chem. Soc. Rev.*, 2017, **46**, 4895.
30 M. Patra, K. Zarschler, H.-J. Pietzsch, H. Stephan and G. Gasser, New insights into the pretargeting approach to image and treat tumours, *Chem. Soc. Rev.*, 2016, **45**(23), 6415–6431.
31 O. Keinanen, K. Fung, J. M. Brennan, N. Zia, M. Harris, E. van Dam, C. Biggin, A. Hedt, J. Stoner, P. S. Donnelly, J. S. Lewis and B. M. Zeglis, Harnessing (64)Cu/(67)Cu for a theranostic approach to pretargeted radioimmunotherapy, *Proc. Natl. Acad. Sci. U. S. A.*, 2020, **117**(45), 28316–28327.

32 U. M. Battisti, K. Bratteby, J. T. Jorgensen, L. Hvass, V. Shalgunov, H. Mikula, A. Kjaer and M. M. Herth, Development of the First Aliphatic (18)F-Labeled Tetrazine Suitable for Pretargeted PET Imaging-Expanding the Bioorthogonal Tool Box, *J. Med. Chem.*, 2021, **64**(20), 15297–15312.

33 E. J. L. Stéen, J. T. Jørgensen, C. Denk, U. M. Battisti, K. Nørregaard, P. E. Edem, K. Bratteby, V. Shalgunov, M. Wilkovitsch, D. Svatunek, C. B. M. Poulie, L. Hvass, M. Simón, T. Wanek, R. Rossin, M. Robillard, J. L. Kristensen, H. Mikula, A. Kjaer and M. M. Herth, Lipophilicity and Click Reactivity Determine the Performance of Bioorthogonal Tetrazine Tools in Pretargeted In Vivo Chemistry, *ACS Pharmacol. Transl. Sci.*, 2021, **4**(2), 824–833.

34 H. Mutlu, E. B. Ceper, X. Li, J. Yang, W. Dong, M. M. Ozmen and P. Theato, Sulfur Chemistry in Polymer and Materials Science, *Macromol. Rapid Commun.*, 2019, **40**(1), 1800650.

35 S. R. Banerjee, C. A. Foss, M. Castanares, R. C. Mease, Y. Byun, J. J. Fox, J. Hilton, S. E. Lupold, A. P. Kozikowski and M. G. Pomper, Synthesis and Evaluation of Technetium-99m- and Rhenium-Labeled Inhibitors of the Prostate-Specific Membrane Antigen (PSMA), *J. Med. Chem.*, 2008, **51**(15), 4504–4517.